Quantum theory of isomeric excitation of ^{229}Th in strong laser fields

Wu Wang[1] and Xu Wang[1,2,*]

[1]*Graduate School, China Academy of Engineering Physics, Beijing 100193, China*

[2]*Southern Center for Nuclear-Science Theory, Institute of Modern Physics, Chinese Academy of Sciences, Huizhou, Guangdong 516000, China*

(Received 26 June 2022; revised 18 June 2023; accepted 21 November 2023; published 12 December 2023)

A general quantum mechanical theory is developed for the isomeric excitation of ^{229}Th in strong femtosecond laser pulses. The theory describes the tripartite interaction between the nucleus, the atomic electrons, and the laser field. The nucleus can be excited both by the laser field and by laser-driven electronic transitions. Numerical results show that strong femtosecond laser pulses are very efficient in exciting the ^{229}Th nucleus, yielding nuclear excitation probabilities on the order of 10^{-11} per nucleus per pulse. Laser-driven electronic excitations are found to be more efficient than direct optical excitations.

DOI: 10.1103/PhysRevResearch.5.043232

I. INTRODUCTION

Nuclear isomers are nuclear metastable states with relatively long half-lives. They have important applications in energy storage [1–5], medical imaging [6], nuclear structure elucidation [7], etc. One of the most fascinating nuclear isomers of substantial recent interest is the ^{229}Th isomer, which has an extremely low energy of only about 8 eV above the nuclear ground state [8–17]. It has been proposed as a nuclear clock [18–26] that may outperform or complement today's atomic clocks.

One of the current research focuses is to find efficient methods to excite the ^{229}Th nucleus from the ground state to the isomeric state [27–46]. Existing methods or proposals may be summarized into the following categories: optical excitation (OE), electronic excitation (EE), or laser-driven electronic excitation (LDEE). OE using vacuum ultraviolet light around 8 eV is conceptually straightforward, however, several experimental attempts have given negative results [27–30], possibly due to inaccurate knowledge of the isomeric energy. An indirect OE method was demonstrated [31] using 29-keV synchrotron radiations to pump the nucleus to the second excited state which then decays preferably into the isomeric state [32]. Several EE processes are discussed and calculated, including nuclear excitation by inelastic electron scattering [33–35], by bound electronic transition or by electron capture [36]. For the LDEE category, electronic bridge (EB) schemes are most discussed [37–43]. The EB method has not been experimentally realized due to the requirements on resonant conditions for both nuclear and electronic transitions.

The possibility of using strong femtosecond laser pulses for the isomeric excitation has been considered by us previously [47,48]. We explain that efficient isomeric excitation of ^{229}Th can be achieved through a laser-driven electron recollision process: (i) An outer electron is pulled out by the strong laser field, (ii) the electron is driven away but has a probability to be driven back and recollide with its parent ion core when the oscillating laser field reverses its direction, and (iii) the recolliding electron excites the ^{229}Th nucleus from the ground state to the isomeric state. This electron recollision process is well-known [49–51] and is the core process underlying strong-field phenomena including high harmonic generation [52–54], nonsequential double ionization [55–57], laser-induced electron diffraction [58–60], attosecond pulse generation [61–64], etc. Therefore, this recollision-induced-nuclear-excitation (RINE) process is an interesting combination of ^{229}Th nuclear physics and strong-field atomic physics [65,66]. Semiclassical calculations show that the probability of isomeric excitation is on the order of 10^{-12} per femtosecond laser pulse per nucleus [48].

In this paper, we go further by developing a quantum mechanical theory for the isomeric excitation process by strong femtosecond laser fields. Such a theory is desirable for a couple reasons. First, it provides a quantum basis for the RINE process and benchmarks for our previous semiclassical calculations. Second, it provides a more complete picture of isomeric excitation in strong laser fields by including processes beyond RINE. The RINE involves only laser-driven free-free electronic transitions, whereas the quantum theory also includes intrinsically laser-driven free-bound and bound-bound electronic transitions. The quantum theory describes the tripartite interaction between the nucleus, the atomic electrons, and the laser field. It simultaneously encloses OE and LDEE channels, so direct comparisons between these channels are possible for given laser parameters.

This paper is organized as follows. In Sec. II, the tripartite quantum theory is developed. Numerical results of nuclear excitation probabilities under different laser parameters are

*Corresponding author: xwang@gscaep.ac.cn

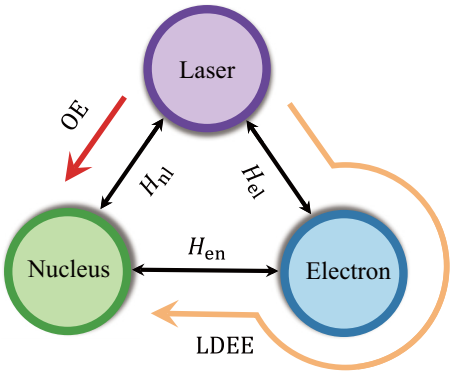

FIG. 1. Illustration of the tripartite interaction between the nucleus, the atomic electrons, and the laser field. The nucleus can be excited by both the OE channel and the LDEE channel.

given in Sec. III. Further discussions are given in Sec. IV, and a conclusion is given in Sec. V.

II. THE QUANTUM THEORY

A. The tripartite interaction

The Hamiltonian of the laser-nucleus-electron system can be written as

$$H = H_{\rm e} + H_{\rm n} + H_{\rm en} + H_{\rm el} + H_{\rm nl}\,, \tag{1}$$

where the Hamiltonians on the right-hand side are, respectively, for the atomic electrons, the nucleus, the electron-nucleus coupling, the electron-laser coupling, and the nucleus-laser coupling. They describe the tripartite interaction between the nucleus, the atomic electrons, and the laser field, as illustrated in Fig. 1. The state space of $H_{\rm e}$ is the atomic eigenstate, including both bound and continuum states, which are denoted by $|\varphi_i\rangle$. The state space of $H_{\rm n}$ contains the nuclear ground state $|I_g M_g\rangle$ and the isomeric excited state $|I_e M_e\rangle$. The electron-nucleus coupling $H_{\rm en}$ is given as a summation over irreducible tensor operators [67]

$$H_{\rm en} = \sum_{\tau=E,M}\sum_{lm}(-1)^m \mathcal{M}^{\tau}_{l-m} T^{\tau}_{lm}\,, \tag{2}$$

where $\mathcal{M}^{\tau}_{lm}$ is the nuclear multipole moment of type τ (E for electric, M for magnetic) and rank l. T^{τ}_{lm} is the corresponding multipole operator for the atomic electrons and is given by

$$\begin{aligned} T^{E}_{lm} &= \sqrt{\frac{4\pi}{2l+1}}\int \frac{\rho_{\rm e}(\boldsymbol{r})}{r^{l+1}} Y_{lm}(\theta,\phi)d\tau,\\ T^{M}_{lm} &= \sqrt{\frac{4\pi}{2l+1}}\int \frac{i}{cl}\frac{\boldsymbol{j}_{\rm e}(\boldsymbol{r})\cdot\boldsymbol{L}[Y_{lm}(\theta,\phi)]}{r^{l+1}} d\tau, \end{aligned} \tag{3}$$

where $Y_{lm}(\theta,\phi)$ is spherical harmonics and $\rho_{\rm e}(\boldsymbol{r})$ and $\boldsymbol{j}_{\rm e}(\boldsymbol{r})$ are charge and current density operators for the electron.

The nucleus-laser coupling is given by

$$H_{\rm nl} = -\frac{1}{c}\int \boldsymbol{j}_n(\boldsymbol{r})\cdot\boldsymbol{A}(\boldsymbol{r},t)d\tau, \tag{4}$$

where $\boldsymbol{j}_n(\boldsymbol{r})$ and $\boldsymbol{A}(\boldsymbol{r},t)$ are the operators for the nuclear current density and laser vector potential, respectively. The vector potential $\boldsymbol{A}(\boldsymbol{r},t)$ satisfies the Coulomb gauge $\nabla\cdot\boldsymbol{A}(\boldsymbol{r},t)=0$. Assume the vector potential has the following form:

$$\boldsymbol{A}(\boldsymbol{r},t) = \frac{\hat{\boldsymbol{z}}}{2}[w(t)\exp(i\boldsymbol{k}\cdot\boldsymbol{r}) + \text{c.c.}], \tag{5}$$

where $w(t)$ is a temporal function, $\boldsymbol{k}$ and $\hat{\boldsymbol{z}}$ are the wave vector and the polarization unit vector. By expanding the vector potential in vector spherical harmonics, the nucleus-laser coupling can be rewritten as

$$H_{\rm nl} = -\sqrt{4\pi}\sum_{\tau=E,M}\sum_{lm}\sqrt{2l+1}(-1)^m \mathcal{M}^{\tau}_{l-m} C^{\tau}_{lm}\,, \tag{6}$$

where C^{τ}_{lm} is the multipole expansion coefficient of the vector potential

$$\begin{aligned} C^{E}_{lm} &= \frac{ik^{l-1}k_0}{(2l+1)!!}\sqrt{\frac{l+1}{l}}[w(t)i^{l-1}+\text{c.c.}]\frac{\hat{\boldsymbol{z}}}{2}\cdot\boldsymbol{A}^{\rm E}_{lm}(\hat{\boldsymbol{k}})\,,\\ C^{M}_{lm} &= \frac{-ik^{l}}{(2l+1)!!}\sqrt{\frac{l+1}{l}}[w(t)i^{l}+\text{c.c.}]\frac{\hat{\boldsymbol{z}}}{2}\cdot\boldsymbol{A}^{\rm M}_{lm}(\hat{\boldsymbol{k}})\,. \end{aligned} \tag{7}$$

Here $k_0=\omega_0/c$ with ω_0 the nuclear energy gap, and $\hat{\boldsymbol{k}}=\boldsymbol{k}/k$ is the unit vector along the $\boldsymbol{k}$ direction. $\boldsymbol{A}^{\tau}_{lm}(\hat{\boldsymbol{k}})$ is the transverse vector spherical harmonics [68],

$$\begin{aligned} \boldsymbol{A}^{E}_{lm}(\hat{\boldsymbol{k}}) &= \frac{k}{\sqrt{l(l+1)}}\nabla Y_{lm}(\hat{k}),\\ \boldsymbol{A}^{M}_{lm}(\hat{\boldsymbol{k}}) &= \frac{1}{\sqrt{l(l+1)}}\boldsymbol{L}Y_{lm}(\hat{k}), \end{aligned} \tag{8}$$

with the orthonormal relation

$$\int \boldsymbol{A}^{\tau}_{lm}(\hat{\boldsymbol{k}})\cdot\boldsymbol{A}^{\tau'*}_{l'm'}(\hat{\boldsymbol{k}})d\Omega_{\hat{\boldsymbol{k}}} = \delta_{ll'}\delta_{mm'}\delta_{\tau\tau'}. \tag{9}$$

A similar expression for the multipole expansion of the nucleus-laser coupling has also been given in Ref. [69] by using rotation matrices.

Similar to the nucleus-laser coupling, the electron-laser coupling can also be expressed as a summation of multipole terms. However, the dipole approximation is usually sufficient, in which only the electric dipole interaction is used to describe the electron dynamics in the laser field. In the approximation, the electron-laser coupling is written as

$$H_{\rm el} = -\boldsymbol{D}\cdot\boldsymbol{E}(t). \tag{10}$$

Here $\boldsymbol{D}$ is the dipole moment operator, and $\boldsymbol{E}(t)$ is the laser electric field at the position of the atom: $\boldsymbol{E}(t)\equiv\boldsymbol{E}(\boldsymbol{r}=\boldsymbol{0},t) = -\partial\boldsymbol{A}(\boldsymbol{r}=\boldsymbol{0},t)/\partial t$. Note that the dipole approximation in $H_{\rm el}$ does not affect the energy exchange mechanism between the atomic electrons and the nucleus, which is described by $H_{\rm en}$ and is of type magnetic dipole ($M1$) or electric quadrupole ($E2$) for ^{229}Th isomers.

B. The nuclear excitation probability

Without the laser field, the Hamiltonian of the nucleus-electron system is

$$H_0 = H_{\rm e} + H_{\rm n} + H_{\rm en}, \tag{11}$$

with eigenstates

$$H_0|\Psi_{\mu,\varepsilon}\rangle = E_{\mu,\varepsilon}|\Psi_{\mu,\varepsilon}\rangle, \tag{12}$$

where μ (ε) denotes the nuclear state (electronic state). For example, $\mu = g$ or e for the nuclear ground state or the isomeric excited state, and $\varepsilon = i$ or f for the initial or the final electronic state. The eigenstate $|\Psi_{\mu,\varepsilon}\rangle$ can be expanded using the uncoupled states $|I_\mu M_\mu, \varphi_\varepsilon\rangle \equiv |I_\mu M_\mu\rangle \otimes |\varphi_\varepsilon\rangle$ using perturbation theory

$$|\Psi_{\mu,\varepsilon}\rangle = |I_\mu M_\mu, \varphi_\varepsilon\rangle + \sum_{\mu',\varepsilon'} |I_{\mu'} M_{\mu'}, \varphi_{\varepsilon'}\rangle \times \frac{\langle I_{\mu'} M_{\mu'}, \varphi_{\varepsilon'}|H_{\rm en}|I_\mu M_\mu, \varphi_\varepsilon\rangle}{E_\varepsilon - E_{\varepsilon'} + E_\mu - E_{\mu'}}, \tag{13}$$

where E_ε and E_μ are the energy eigenvalues corresponding to the atomic state $|\varphi_\varepsilon\rangle$ and nuclear state $|I_\mu M_\mu\rangle$, respectively. One notes from Eq. (13) that due to the presence of electron-nucleus coupling $H_{\rm en}$, the mixing between the nuclear ground state and the isomeric state occurs. This is known as the nuclear hyperfine mixing effect, which is particularly pronounced in highly charged ions [70–76].

Initially, at time t_0, the nucleus-electron system is assumed to be in its ground state $|\Psi_{g,i}\rangle$. Then the probability of nuclear isomeric excitation at a later time $t > t_0$ is given by

$$P_{\rm exc}(t) = \sum_f |\langle \Psi_{e,f}|U(t,t_0)|\Psi_{g,i}\rangle|^2 , \tag{14}$$

where $U(t,t_0)$ is the time evolution operator in the Schrödinger picture corresponding to the total Hamiltonian H, and the summation runs over all final electronic states.

The time evolution is computationally very demanding due to the large state space (which comes mostly from the electronic states). However, one notices that the couplings of the nucleus to the laser field and to the electrons are weak. This allows the usage of perturbative treatments for the laser-nucleus and electron-nucleus couplings, reducing the computation load substantially. The laser-electron coupling, in contrast, is very strong and must be treated nonperturbatively. Using the time-dependent perturbation theory, the time evolution operator $U(t,t_0)$ becomes

$$U(t,t_0) = U_0(t,t_0)e^{-iH_{\rm n}(t-t_0)}[1 - iV_I(t)], \tag{15}$$

where $V_I(t)$ is defined by

$$V_I(t) = \int_{t_0}^{t} e^{-iH_{\rm n}(t_0-t')}U_0(t_0,t')(H_{\rm en} + H_{\rm nl}) \times e^{-iH_{\rm n}(t'-t_0)}U_0(t',t_0)dt'. \tag{16}$$

In the above expressions, $U_0(t,t_0)$ is the time evolution operator corresponding to $(H_{\rm e} + H_{\rm el})$.

Substituting Eqs. (13) and (15) into Eq. (14), $P_{\rm exc}(t)$ can be derived into the following form after averaging over initial nuclear states and summing over final states:

$$P_{\rm exc}(t) = 4\pi \sum_{\tau,l} \frac{B(\tau l, g \to e)}{(2l+1)^2} \sum_{f,m} \left|N_{lm}^{\tau;fi}\right|^2 . \tag{17}$$

Detailed derivations of the above equation can be found in Appendix A. The favorable feature of the above formula is that the nuclear transitions are packed in $B(\tau l, g \to e)$ and the electronic transitions are packed in $N_{lm}^{\tau;fi}$. The former is the reduced nuclear transition probability

$$B(\tau l, g \to e) = \frac{2l+1}{4\pi(2I_g+1)} \sum_{M_e M_g m} \left|\langle I_e M_e|\mathcal{M}_{lm}^{\tau}|I_g M_g\rangle\right|^2$$

and $N_{lm}^{\tau;fi}$, depending only on the electronic initial and final states, is given by

$$\begin{aligned} N_{lm}^{\tau;fi} = &-i\int_{t_0}^{t} \langle\varphi_f(t')|T_{lm}^{\tau}|\varphi_i(t')\rangle e^{i\omega_0 t'}dt' \\ &+ e^{i\omega_0 t}\sum_{kn}\langle\varphi_f(t)|\varphi_n\rangle\frac{\langle\varphi_n|T_{lm}^{\tau}|\varphi_k\rangle}{E_n - E_k + \omega_0}\langle\varphi_k|\varphi_i(t)\rangle \\ &+ e^{i\omega_0 t_0}\frac{\langle\varphi_f|T_{lm}^{\tau}|\varphi_i\rangle}{E_i - E_f - \omega_0} \\ &+ i\delta_{fi}\sqrt{4\pi(2l+1)}\int_{t_0}^{t} C_{lm}^{\tau}(t')e^{i\omega_0 t'}dt' . \end{aligned} \tag{18}$$

In the above formula, $|\varphi_{i/f}(t)\rangle$ is the electronic state evolved by $U_0(t,t_0)$ from the state $|\varphi_{i/f}\rangle$. Note that both LDEE and OE channels emerge. The first three lines of Eq. (18) all contain the (time-dependent) electronic states and they describe the LDEE channel. As the atomic state space includes both bound and free states, the contributions from bound-bound, bound-free, and free-free electronic transitions to the nuclear excitation are taken into account intrinsically. The last line, which does not contain electronic states, describes the OE channel, with the C_{lm}^{τ} given in Eq. (7). The OE channel does not change the electronic state, hence the δ_{fi}.

For the ^{229}Th nucleus, the leading nuclear transitions from the ground state to the isomeric state are $M1$ and $E2$. In our calculation we use the reduced transition probability values $B(M1, e \to g) = 0.005$ W.u. and $B(E2, e \to g) = 30$ W.u., as predicted recently by Minkov and Pálffy [77].

C. The time-dependent ZORA equation

The dynamics of the atomic electrons driven by a strong laser pulse has been extensively studied in strong-field atomic physics. Theoretically, most strong-field phenomena can be well understood by solving the time-dependent Schrödinger equation under a single-active-electron (SAE) approximation [50,51,78–81], which assumes that only the outermost electron actively responds to the external laser field, with the remaining electrons contributing a mean-field potential.

The difference between the current work and traditional strong-field atomic physics is the addition of the nuclear degree of freedom. We find that this difference makes the Schrödinger equation insufficient. The main contribution to nuclear excitation comes from electron wave functions very close (around 10^{-2} a.u.) to the nucleus due to the factor r^{-l-1} in the electronic operator T_{lm}^{τ} of Eq. (3). Yet the amplitudes of the Schrödinger wave functions, even for low electron energies, can be very different from those of the Dirac wave functions in this region due to the high nuclear charge ($Z = 90$). Therefore, relativistic effects are important for the isomeric excitation. A similar conclusion has also been given in nuclear excitation by inelastic electron scattering [35].

The straight way to calculate the nuclear excitation probability is to solve the time-dependent Dirac equation, which,

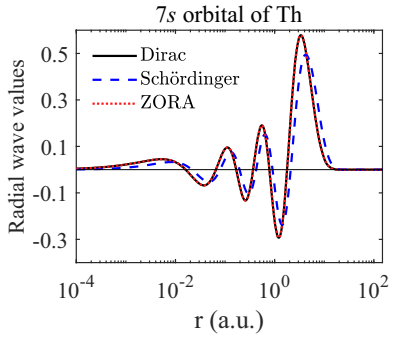

FIG. 2. Radial wave function of the $7s$ orbital of the ^{229}Th atom, calculated by three different Hamiltonians as labeled. The ZORA wave function is almost identical to the Dirac one, and the two can barely be visually distinguished.

however, is very time consuming. Here we instead use an alternative and much more economical approach. We adopt for H_e a so-called zero-order-regular-approximation (ZORA) Hamiltonian [82–84], instead of the Dirac Hamiltonian. The ZORA Hamiltonian is an effective two-component Hamiltonian giving an accurate approximation of relativistic effects:

$$H_{\rm ZORA} = \boldsymbol{\sigma}\cdot\boldsymbol{p}\frac{1}{2-\alpha^2 V(r)}\boldsymbol{\sigma}\cdot\boldsymbol{p} + V(r), \tag{19}$$

where $\boldsymbol{\sigma}$ is the Pauli matrix, α is the fine structure constant, and $V(r)$ is a central potential felt by the electron.

Figure 2 shows the radial wave function of the $7s$ orbital of the ^{229}Th atom for the Schrödinger case, the (large component of the) Dirac case, and the ZORA case. One can see that the ZORA wave function is almost identical to the Dirac one, whereas the Schrödinger wave function has smaller amplitudes close to the nucleus, leading to an underestimation of the nuclear excitation probability up to an order of magnitude. The potential energy $V(r)$ used in Fig. 2 and in the results below is calculated by the RADIAL package [85] based on a self-consistent Dirac-Hartree-Fock-Slater method.

The temporal evolution of the electronic state $|\varphi_i(t)\rangle$ obeys the time-dependent ZORA equation:

$$i\frac{\partial}{\partial t}|\varphi_i(t)\rangle = [H_{\rm ZORA} + H_{\rm el}(t)]|\varphi_i(t)\rangle\,. \tag{20}$$

The laser electric field is assumed to be linearly polarized along the z axis with amplitude F_0, envelope function $f(t)$, and angular frequency ω. Thus, the dipole coupling between the laser and the active electron is written as $H_{\rm el}(t) = zF_0 f(t)\sin\omega t$. Equation (20) is numerically solved using a generalized pseudospectral method [86–88]. The time propagation of the ZORA equation can be realized using a split-operator method

$$\begin{aligned}|\varphi_i(t+dt)\rangle = {}& \exp(-iH_{\rm ZORA}dt/2)\\ &\times\ \exp[-iH_{\rm el}(t+dt/2)dt]\\ &\times\ \exp(-iH_{\rm ZORA}dt/2)|\varphi_i(t)\rangle + O(dt^3),\end{aligned} \tag{21}$$

where dt is the time step. From the above equation, the time evolution of the wave function from t to $t+dt$ is completed by three steps: (i) evolution for a half-time step $dt/2$ in the energy space spanned by $H_{\rm ZORA}$, and (ii) evolution for one time step dt in the coordinate space under the influence of the electron-laser coupling $H_{\rm el}$, and (iii) evolution for another half-time step $dt/2$ in the energy space spanned by $H_{\rm ZORA}$. In contrast to Refs. [86–88], here the wave function at time t is expanded in spherical spinors rather than spherical harmonics for adapting the ZORA Hamiltonian

$$|\varphi_i(t)\rangle = \sum_{|\kappa|\leqslant K_{\rm max}} |R_\kappa(r,t)\rangle|\Omega_{\kappa m}(\theta,\phi)\rangle, \tag{22}$$

where $|R_\kappa(r,t)\rangle$ is the (time-dependent) radial wave function, $|\Omega_{\kappa m}(\theta,\phi)\rangle$ is spherical spinors [68] with quantum number κ and magnetic quantum number m, and $K_{\rm max}$ is an integer to truncate the orbital angular momentum. Here, m is fixed due to $\Delta m = 0$ in the linearly polarized laser field. Spherical spinors $|\Omega_{\kappa m}(\theta,\phi)\rangle$ are orthonormal,

$$\langle\Omega_{\kappa m}|\Omega_{\kappa' m'}\rangle = \delta_{\kappa\kappa'}\delta_{mm'}, \tag{23}$$

and they satisfy the eigenvalue equation:

$$(-1-\boldsymbol{\sigma}\cdot\boldsymbol{L})|\Omega_{\kappa m}(\theta,\phi)\rangle = \kappa|\Omega_{\kappa m}(\theta,\phi)\rangle. \tag{24}$$

The calculation is performed in a spherical box with radius 150 a.u. and 300 spatial grid points (nonuniform grid, denser near the origin). The time step is $dt = 0.1$ a.u. The orbital angular momentum is truncated at $K_{\rm max} = 80$ in the partial-wave expansion of Eq. (22). A boundary absorbing function $1/[1+\exp(br-r_0)]$ with $b = 1.25$ and $r_0 = 120$ a.u. is used to avoid boundary reflection. The convergency has been carefully checked by varying the calculation parameters. The initial state $|\varphi_i\rangle$ for the first, second, third, and fourth electrons sequentially pulled out by the laser field is the $7s_{1/2}$ orbital of the Th atom, the $7s_{1/2}$ orbital of the Th^+ ion, the $6d_{5/2}$ orbital of the Th^{2+} ion, and the $5f_{5/2}$ orbital of the Th^{3+} ion, respectively. The magnetic quantum number m is fixed at $1/2$.

III. NUMERICAL RESULTS

With the time evolution of the electronic states numerically solved, we can calculate the nuclear excitation probability $P_{\rm exc}(t)$ using Eqs. (17) and (18). In this section, we present $P_{\rm exc}(t)$ with different laser wavelengths, laser pulse durations, and laser intensities. Comparisons between OE and LDEE channels and discussions about effect of uncertainty of the isomeric energy are also presented.

A. Excitation probability under two wavelengths

Figure 3 shows the nuclear excitation probability $P_{\rm exc}(t)$ during a laser pulse for two different laser wavelengths, namely, 800 nm and 400 nm. For both cases, the laser pulse has a duration of five optical cycles with a temporal envelop function $f(t) = \sin^2(\pi t/NT)$, where $T = 2\pi/\omega$ is the period and $N = 5$ is the number of optical cycles. The peak intensity of the laser pulse is 10^{14} W/cm^2. This intensity has the ability to drive the outermost three electrons of the Th atom, with negligible effects on the fourth electron, which lies too deeply (a higher intensity is needed to drive this electron, as shown in an example later). Based on the SAE approximation, we

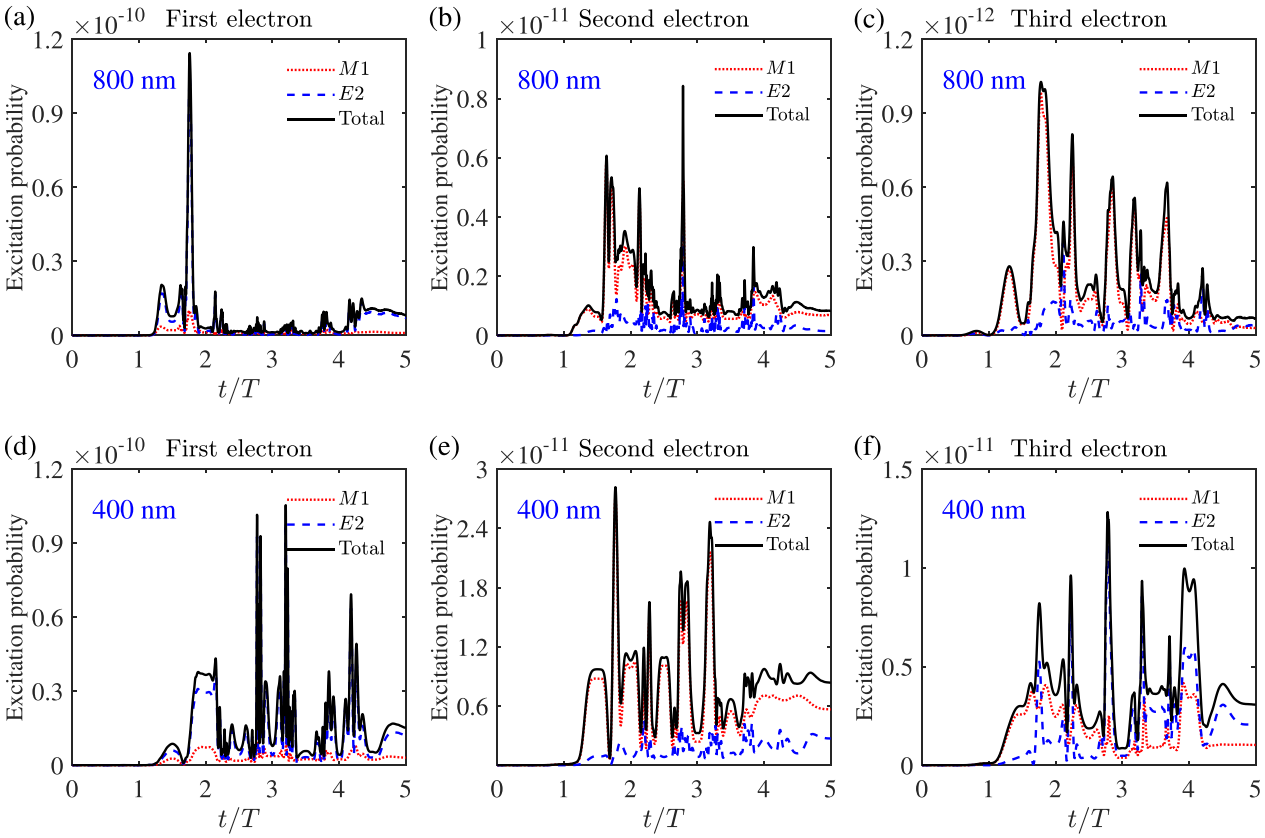

FIG. 3. Nuclear excitation probability $P_{\rm exc}(t)$ during a laser pulse for the first electron (left column), second electron (middle column), and third electron (right column). Two different laser wavelengths are used, namely, 800 nm (top row) and 400 nm (bottom row). For both wavelengths, the laser pulse has a sine-squared shape with peak intensity 10^{14} W/cm^2. Separated contributions from the $M1$ and the $E2$ channels are also shown, as labeled.

calculate separately the first, second, and third electrons. For each case, the total excitation probability as well as separated contributions from the $M1$ or $E2$ channels are presented.

With these laser parameters, contributions from the OE channel are found to be three to four orders of magnitude lower than those from the LDEE channel. This is due to the fact that both 800 nm (photon energy 1.55 eV) and 400 nm (photon energy 3.10 eV) are far off resonance to the nuclear energy gap of 8.28 eV, albeit with a high intensity. Therefore, the excitation probabilities presented in Fig. 3 are almost solely from LDEE. For 800 nm, the end-of-pulse nuclear excitation probability is about 8.2×10^{-12}, 8.3×10^{-13}, and 6.7×10^{-14} for the first, second, and third electrons, respectively. The total excitation probability is about 9.1×10^{-12}. For 400 nm, the end-of-pulse nuclear excitation probability is about 1.5×10^{-11}, 8.4×10^{-12}, and 3.1×10^{-12} for the first, second, and third electrons, respectively. The total excitation probability is about 2.7×10^{-11}. This is about three times higher than the 800-nm case.

The relative importance between $M1$ and $E2$ varies from case to case. One sees from the first electron that $E2$ is more important than $M1$ almost for the entire pulse, for both 800 nm and 400 nm. However, the situation reverses for the second electron, where $M1$ dominates during the entire pulse. The situation for the third electron is different for 800 nm and 400 nm. For 800 nm, $M1$ dominates most of the time during the pulse, but near the end of the pulse, the two have almost equal contributions to nuclear excitation. For 400 nm, in contrast, $E2$ dominates for most of the pulse duration except for the initial stage. These results have no simple interpretations but they can be attributed to the dependency of the matrix element of T^{τ}_{lm} on the time-dependent electronic states.

B. Excitation with different pulse durations

In Fig. 4, we show the nuclear excitation probability $P_{\rm exc}(t)$ with laser pulses of different durations ($N = 10$ and 15 optical cycles). The wavelength and intensity of the laser pulses are fixed at 400 nm and 10^{14} W/cm^2, so this figure is to be compared with the lower row of Fig. 3, which is for a shorter pulse of $N = 5$. The outermost three electrons contribute to the nuclear excitation and are calculated separately.

For the case of $N = 10$, the end-of-pulse nuclear excitation probability is about 3.5×10^{-12}, 7.0×10^{-12}, and 1.5×10^{-12} for the first, second, and third electrons, respectively. The total excitation probability is about 1.2×10^{-11}.

For the case of $N = 15$, the end-of-pulse nuclear excitation probability is about 2.7×10^{-12}, 7.4×10^{-12}, and 1.7×10^{-12} for the first, second, and third electrons, respectively. The total excitation probability is about 1.2×10^{-11}, almost identical to the $N = 10$ case. This value is about two times lower than the $N = 5$ case shown above (Fig. 3).

Another noticeable difference is that for $N = 5$, the first electron contributes the most to the nuclear excitation,

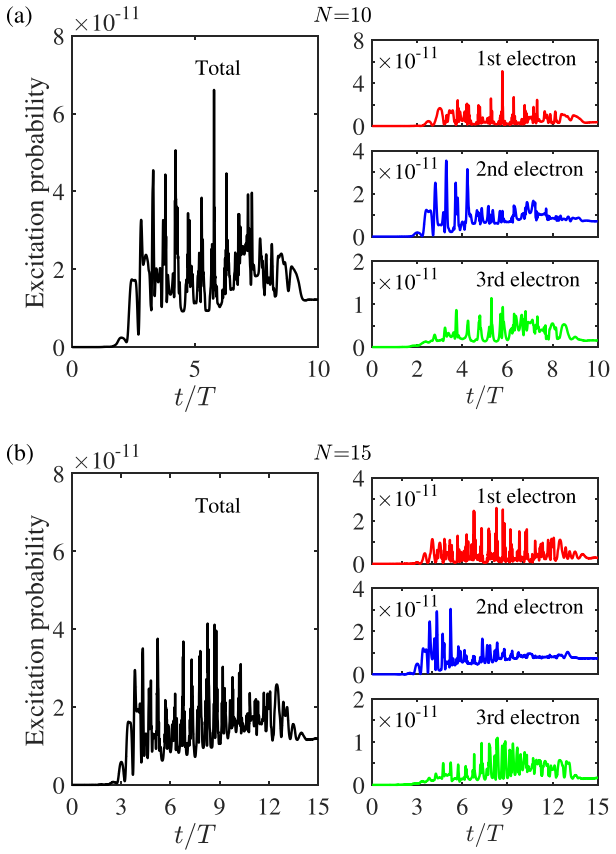

FIG. 4. Nuclear excitation probability $P_{\rm exc}(t)$ during a laser pulse of duration (a) $N = 10$ optical cycles and (b) $N = 15$ optical cycles. The laser wavelength is 400 nm and the peak intensity is 10^{14} W/cm^2. For each case, separated contributions from the outermost three electrons are also shown.

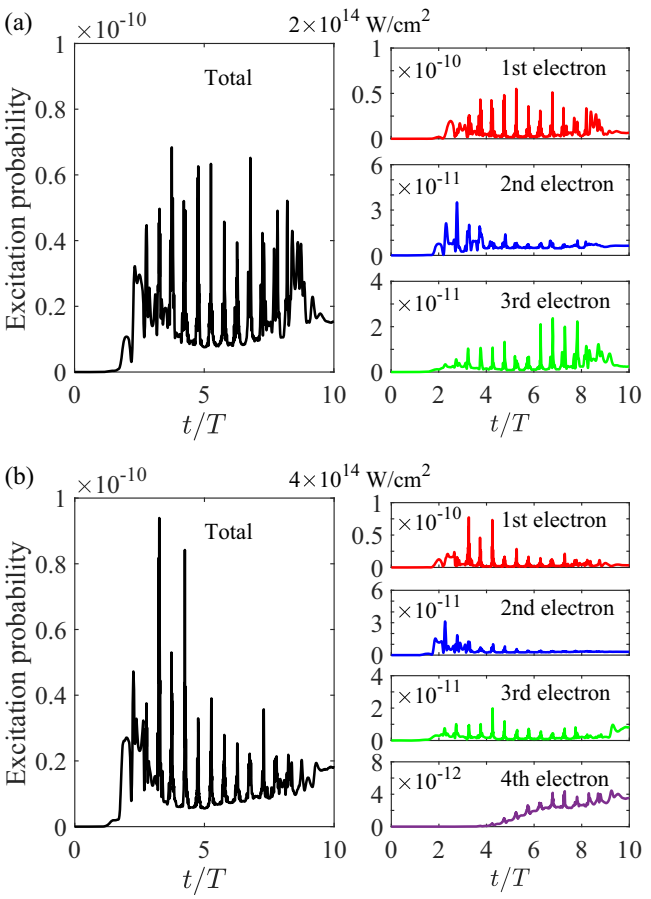

FIG. 5. Nuclear excitation probability $P_{\rm exc}(t)$ during a laser pulse with intensity (a) 2×10^{14} W/cm^2 and (b) 4×10^{14} W/cm^2. The laser wavelength is 400 nm and the duration is ten optical cycles. For the higher intensity, the fourth electron starts to contribute to nuclear excitation.

whereas for $N = 10$ or 15 the second electron contributes the most. The major difference from the longer pulses is to reduce the contribution from the first electron (from 1.5×10^{-11} for $N = 5$, to 3.5×10^{-12} for $N = 10$ and 2.7×10^{-12} for $N = 15$). Without presenting analyses involving too many details, this pulse-duration effect can be briefly understood as follows: The shorter pulse provides a larger bandwidth such that it drives the first electron to favorable states for the nuclear excitation. Longer pulses reduce the bandwidth and diminish electronic transitions to these favorable states. Nevertheless, the pulse-duration effect is not severe: Under the same peak intensity, pulses with different durations lead to nuclear excitation probabilities within a factor of 2 or 3.

C. Excitation with different laser intensities

Figure 5 shows the nuclear excitation probability during two pulses of different peak intensities, namely, 2×10^{14} and 4×10^{14} W/cm^2. Both laser pulses have wavelength 400 nm and duration ten optical cycles. With the lower intensity, the first three electrons contribute to the nuclear excitation, whereas with the higher intensity, the fourth electron starts to contribute to the nuclear excitation.

For the lower intensity, the end-of-pulse nuclear excitation probability is about 6.5×10^{-12}, 6.4×10^{-12}, and 2.5×10^{-12} for the first, second, and third electron, respectively. The total nuclear excitation probability is about 1.5×10^{-11}.

For the higher intensity, the end-of-pulse nuclear excitation probability is about 3.5×10^{-12}, 3.0×10^{-12}, 8.0×10^{-12}, and 3.5×10^{-12} for the first, second, third, and fourth electrons, respectively. The total nuclear excitation probability is about 1.8×10^{-11}. From Figs. 4(a) and 5, one can see that the total nuclear excitation probability increases with the laser intensity.

D. OE vs LDEE channels

In all the above results, the LDEE channel dominates the nuclear excitation, and the OE channel is weaker by three or four orders of magnitude. As explained, this is because both 800 nm and 400 nm are far off resonant with the nuclear isomeric energy. The OE channel is important when the laser frequency is close to the isomeric resonance (8.28 eV = 0.304 a.u.). Figure 6(a) shows a few near-resonant examples for peak intensity 10^{14} W/cm^2 and pulse duration 20 optical cycles. The nuclear excitation probability can reach about 10^{-12} for exact resonance, but drops in the presence of a detuning.

However, this does not mean that the LDEE channel is negligible. Figure 6(b) shows the comparison between OE and

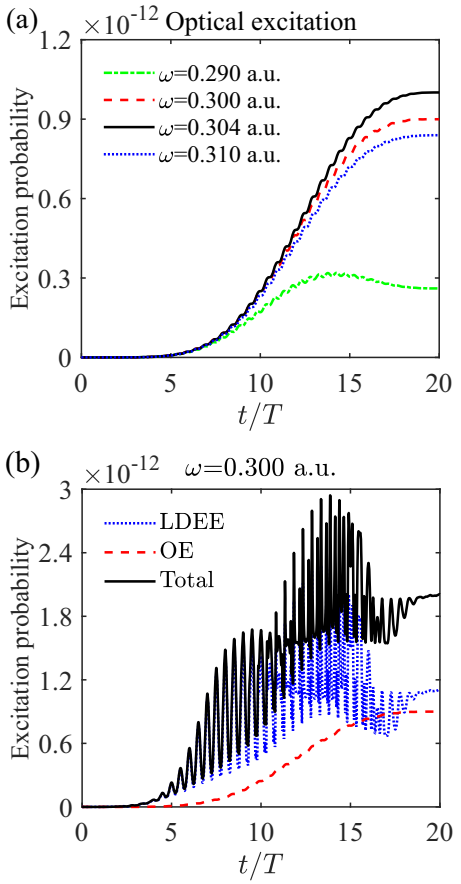

FIG. 6. (a) Nuclear excitation probability $P_{\rm exc}(t)$ from the OE channel for several laser frequencies around the isomeric resonance (8.28 eV = 0.304 a.u.). The laser peak intensity is 10^{14} W/cm^2. (b) Nuclear excitation probability $P_{\rm exc}(t)$ for the Th^{2+} ion with laser frequency 0.300 a.u. (8.16 eV in photon energy) and peak intensity 10^{14} W/cm^2. The OE channel and the LDEE channel lead to comparable nuclear excitation probabilities.

LDEE channels for $\omega = 0.300$ a.u., which is very close to the resonant frequency. The calculation is performed with the Th^{2+} ion. One can see that the two channels are comparable in this example, and the LDEE channel is even higher. Although there is no easy way of obtaining intense laser pulses with photon energies around 8.28 eV, we want to use this example to emphasize that both OE and LDEE processes exist when the ^{229}Th atom is radiated by a laser field, and that it would be dangerous to neglect one of them without doing the calculations. This is why a theory including both channels in a single framework is important.

E. Effect of uncertainty of the isomeric energy

In the above calculations, the isomeric energy ω_0 is fixed at 8.28 eV [12]. However, there is still an uncertainty about 0.17 eV in the measurement. To check the influence of such an uncertainty, the nuclear excitation probability for the Th^{3+} ion is calculated using three different isomeric energies, namely, 8.11 eV, 8.28 eV, and 8.45 eV. The results are shown in Fig. 7. The laser wavelength, pulse duration, and intensity are 400 nm, 10 optical cycles, and 4×10^{14} W/cm^2, respectively.

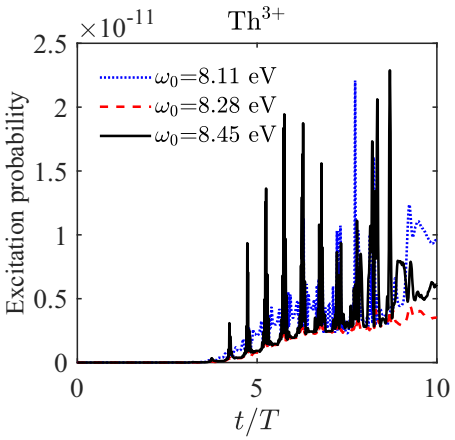

FIG. 7. Nuclear excitation probability $P_{\rm exc}(t)$ for the Th^{3+} ion calculated using three different isomeric energies, as labeled on figure. The laser wavelength is 400 nm, the peak intensity is 4×10^{14} W/cm^2, and the duration is ten optical cycles.

The end-of-pulse nuclear excitation probability is 9.6×10^{-12}, 3.5×10^{-12}, and 6.1×10^{-12} for the three isomeric energies, respectively. The nuclear excitation probability remains within a factor of 3.

We emphasize that the nuclear excitation process in strong femtosecond laser pulses is very different from that in weak continuous-wave laser lights. In strong laser fields, the electron dynamics involves both bound and continuum states, so the electronic transitions have broad energy distributions. In continuous laser lights, the electron dynamics involves only a few (typically two) bound states, so the electronic transitions have narrow energy distributions. Therefore, excitation methods based on continuous lights depend very sensitively on the isomeric energy, whereas our method does not.

IV. DISCUSSION

In Ref. [48], a semiclassical method is used to calculate the nuclear excitation probability based on the recollision picture (i.e., the RINE process). A probability of 4×10^{-12} is obtained for laser wavelength 800 nm and peak intensity 10^{14} W/cm^2. In the full quantum calculation given in this paper (Fig. 3), an excitation probability of 9.1×10^{-12} is obtained for the same wavelength and peak intensity, although with a shorter pulse duration due to the demanding computational load. On the one hand, this indicates that the semiclassical calculation is fairly accurate, giving at least the right order of magnitude. On the other hand, we emphasize that the quantum calculation includes processes that are absent in RINE. RINE only includes laser-driven free-free electronic transitions, whereas the quantum calculation also includes laser-driven free-bound and bound-bound electronic transitions.

From the quantum calculations in this paper, a strong femtosecond laser pulse leads to typical nuclear excitation probabilities on the order of 10^{-11} per nucleus. This is to be compared with the 29-keV indirect OE method, which gives an excitation probability on the order of 10^{-11} per nucleus per second [31]. That is, a femtosecond laser pulse generates

a similar nuclear excitation probability as the (continuous-wave) 29-keV synchrotron radiation does for one second.

Besides the efficiency, our method has the following advantages: (i) Precise knowledge of the isomeric energy is not needed, because the electronic transitions have broad energy distributions which cover the isomeric energy. (ii) Our method is relatively easy to implement experimentally, requiring only tabletop laser systems instead of large facilities. (iii) The excitation is well timed and happens within the short laser pulse. This may be important for future coherent operations of the excitation process.

Our theory applies to isolated atoms or vapors. The number of excited ^{229}Th nuclei from a single laser pulse can be estimated to be $N_{\rm exc} \approx nV_{\rm foc}P_{\rm exc}$, where n is the atomic number density, $V_{\rm foc}$ is the volume of the laser focus, and $P_{\rm exc} \approx 10^{-11}$ is the excitation probability per nucleus. Assuming a Gaussian beam, the focal volume is given by the formula

$$V_{\rm foc} = \frac{16\mathcal{E}^2}{\pi\lambda I^2\tau^2}, \tag{25}$$

where $\mathcal{E}$ is the pulse energy, λ is the wavelength, I is the peak intensity, and τ is the pulse duration. For a pulse with $\mathcal{E} = 0.1$ mJ, $\lambda = 400$ nm, $I = 10^{14}$ W/cm^2, and $\tau = 30$ fs, the focal volume $V_{\rm foc} = 1.4\times10^{-4}$ cm^3. The number density n depends on how the vapor is produced. Usually it can be efficiently produced by thermal vaporization using a relatively weak nanosecond pulse, which do not ionize the metal. The atomic density is usually $n \approx 10^{19}$ cm^{-3} at the metal surface but drops with the vertical distance [89,90]. If we use $n \approx 10^{18}$ cm^{-3}, an order of magnitude smaller than the surface density, then $N_{\rm exc}$ can be estimated to be 1.4×10^3 per pulse.

We emphasize that laser excitation of ^{229}Th involves tripartite interactions between the nucleus, the atomic electrons, and the laser field. Although in this paper we focus on the interaction of ^{229}Th atoms (ions) with a strong femtosecond laser pulse, our theory has more general applicabilities: It provides a general theoretical framework for laser excitation of atomic nuclei. Our theory is also applicable to nuclear excitation by a weak continuous laser light. This is an EB process. We show in Appendix B that our theory agrees with existing EB results in this situation.

V. CONCLUSION

In this paper, we consider using strong femtosecond laser pulses to excite the ^{229}Th nucleus. A general quantum mechanical framework is developed to describe the tripartite interaction between the nucleus, the atomic electrons, and the laser field. The nucleus can be excited both by the laser field and by laser-driven electronic transitions. Calculations show that strong femtosecond laser pulses are very efficient in exciting the ^{229}Th nucleus, leading to excitation probabilities on the order of 10^{-11} per nucleus per femtosecond laser pulse. Laser-driven electronic transitions are shown to be more efficient in exciting the nucleus than the laser field itself. The natural and interesting combination between strong-field atomic physics and ^{229}Th nuclear physics leads to a very efficient nuclear excitation method.

ACKNOWLEDGMENT

W.W. acknowledges discussions with Mrs. T. Li and Z. Liu. This work was supported by NSAF Grant No. U2330401 and NSFC Grant No. 12088101.

APPENDIX A: DERIVATION OF EQ. (17)

In this Appendix, we provide more details for the derivation of Eq. (17). The matrix element $\langle\Psi_{e,f}|U(t,t_0)|\Psi_{g,i}\rangle$ can be written in the following form:

$$\begin{aligned}
&\langle\Psi_{e,f}|U(t,t_0)|\Psi_{g,i}\rangle \\
&\quad= -i\langle I_eM_e,\varphi_f|U_0(t,t_0)V_I(t)|I_gM_g,\varphi_i\rangle \\
&\qquad+\sum_{\varepsilon'}\frac{\langle I_eM_e,\varphi_{\varepsilon'}|H_{\rm en}|I_gM_g,\varphi_i\rangle}{E_i-E_{\varepsilon'}-\omega_0}\langle\varphi_f|U_0(t,t_0)|\varphi_{\varepsilon'}\rangle \\
&\qquad+e^{i\omega_0(t-t_0)}\sum_{\varepsilon'}\frac{\langle I_eM_e,\varphi_f|H_{\rm en}|I_gM_g,\varphi_{\varepsilon'}\rangle}{E_f-E_{\varepsilon'}+\omega_0} \\
&\qquad\times\langle\varphi_{\varepsilon'}|U_0(t,t_0)|\varphi_i\rangle.
\end{aligned} \tag{A1}$$

In obtaining the above expression, we have used the perturbation expansions for the initial state $|\Psi_{g,i}\rangle$ and the final state $|\Psi_{e,f}\rangle$ as given in Eq. (13), and $U(t,t_0)$ as given in Eq. (15). Only first-order terms have been kept.

Using the completeness relation of the electronic states $|\varphi_\varepsilon\rangle$, the last line of Eq. (A1) can be written as

$$\begin{aligned}
&\sum_{\varepsilon'}\frac{\langle I_eM_e,\varphi_f|H_{\rm en}|I_gM_g,\varphi_{\varepsilon'}\rangle}{E_f-E_{\varepsilon'}+\omega_0}\langle\varphi_{\varepsilon'}|U_0(t,t_0)|\varphi_i\rangle \\
&\quad=\sum_{\varepsilon',\varepsilon''}\frac{\langle I_eM_e,\varphi_{\varepsilon''}|H_{\rm en}|I_gM_g,\varphi_{\varepsilon'}\rangle}{E_{\varepsilon''}-E_{\varepsilon'}+\omega_0}\langle\varphi_{\varepsilon'}|U_0(t,t_0)|\varphi_i\rangle \\
&\qquad\times\langle\varphi_f|U_0(t,t_0)U_0^\dagger(t,t_0)|\varphi_{\varepsilon''}\rangle.
\end{aligned} \tag{A2}$$

The nuclear excitation probability $P_{\rm exc}(t)$ can be calculated by substituting Eqs. (A1) and (A2) into Eq. (14). It is necessary to trace out all final electronic states. In this situation, we can replace $U_0(t,t_0)|\varphi_f\rangle$ with $|\varphi_f\rangle$ by applying the completeness relation of electronic states again. Then $P_{\rm exc}(t)$ is given by

$$\begin{aligned}
P_{\rm exc}(t)=\sum_f\Bigg|&-i\langle I_eM_e,\varphi_f|V_I(t)|I_gM_g,\varphi_i\rangle \\
&+\frac{\langle I_eM_e,\varphi_f|H_{\rm en}|I_gM_g,\varphi_i\rangle}{E_i-E_f-\omega_0}+e^{i\omega_0(t-t_0)} \\
&\times\sum_{\varepsilon',\varepsilon''}\frac{\langle I_eM_e,\varphi_{\varepsilon''}|H_{\rm en}|I_gM_g,\varphi_{\varepsilon'}\rangle}{E_{\varepsilon''}-E_{\varepsilon'}+\omega_0} \\
&\times\langle\varphi_{\varepsilon'}|U_0(t,t_0)|\varphi_i\rangle\langle\varphi_f|U_0^\dagger(t,t_0)|\varphi_{\varepsilon''}\rangle\Bigg|^2.
\end{aligned} \tag{A3}$$

By using the expression of the electron-nucleus coupling given in Eq. (2) and the Wigner-Eckart theorem, Eq. (17) can be obtained.

APPENDIX B: OBTAINING EB RATE FROM EQ. (17)

Our current paper focuses on describing the nuclear excitation process in a strong femtosecond laser pulse. However, Eq. (17) is also applicable to nuclear excitation by a weak continuous laser light. One immediately notices that this is actually an EB process. Consequently, Eq. (17) should agree with existing EB results in this limit. This is indeed the case, as shown below.

Under the condition of a weak continuous laser field, the time evolution operator $U_0(t,t_0)$ can be expanded as

$$U_0(t,t_0) = e^{-iH_e(t-t_0)} - ie^{-iH_e(t-t_0)} \times \int_{t_0}^{t} e^{-iH_e(t_0-s)} H_{el}(s) e^{iH_e(t_0-s)} ds. \tag{B1}$$

The laser electric field can be taken as the following form:

$$\boldsymbol{E}(t) = \hat{\boldsymbol{z}} F_0 e^{\eta t} \cos\omega t, \tag{B2}$$

where F_0 is the field amplitude, $\hat{\boldsymbol{z}}$ is the polarization direction, and η is a positive small number. Taking t_0 to be $-\infty$, Eq. (B1) is rewritten as

$$U_0(t,t_0) = e^{-iH_e(t-t_0)} + ie^{-iH_e t} F_0 \times \int_{-\infty}^{t} e^{iH_e s} \boldsymbol{D}\cdot\hat{\boldsymbol{z}} e^{\eta s} \cos\omega s\, e^{iH_e(t_0-s)} ds. \tag{B3}$$

Substituting the above equation into Eq. (18) and using the rotating-wave approximation, $N_{lm}^{\tau;fi}$ becomes

$$N_{lm}^{\tau;fi} = \frac{F_0}{2}\sum_k \left[\frac{\langle\varphi_f|T_{lm}^{\tau}|\varphi_k\rangle\langle\varphi_k|\boldsymbol{D}\cdot\hat{\boldsymbol{z}}|\varphi_i\rangle}{\eta + i(E_k - E_i - \omega)} - \frac{\langle\varphi_f|\boldsymbol{D}\cdot\hat{\boldsymbol{z}}|\varphi_k\rangle\langle\varphi_k|T_{lm}^{\tau}|\varphi_i\rangle}{\eta + i(E_f - E_k - \omega)} \right] \times \frac{e^{\eta t + i(E_f - E_i + \omega_0 - \omega)t}}{\eta + i(E_f - E_i + \omega_0 - \omega)}. \tag{B4}$$

Only first-order terms have been kept. The nuclear excitation rate is obtained by

$$\Gamma = \lim_{\eta\to 0}\frac{d}{dt}P_{exc}(t). \tag{B5}$$

Note that Γ no longer has a time dependency as $\eta \to 0$. It follows from Eqs. (17), (B4), and (B5) that

$$\Gamma = 2\pi^2 F_0^2 \sum_{\tau,l,m}\frac{B(\tau l, g\to e)}{(2l+1)^2}\left|\sum_k\left[\frac{\langle\varphi_f|T_{lm}^{\tau}|\varphi_k\rangle}{E_k - E_f - \omega_0}\times\langle\varphi_k|\boldsymbol{D}\cdot\hat{\boldsymbol{z}}|\varphi_i\rangle + \frac{\langle\varphi_f|\boldsymbol{D}\cdot\hat{\boldsymbol{z}}|\varphi_k\rangle}{E_k - E_i + \omega_0}\langle\varphi_k|T_{lm}^{\tau}|\varphi_i\rangle\right]\right|^2 \times \delta(E_f - E_i + \omega_0 - \omega). \tag{B6}$$

Here, the formula $\lim_{\eta\to 0} 2\eta/(\eta^2 + x^2) = 2\pi\delta(x)$ has been used. The Dirac delta function can be eliminated by an integration over the laser angular frequency. For example, the excitation rate for the $M1$ transition can be written explicitly as

$$\Gamma = \frac{64\pi^4 I_s}{9c}B(M1, g\to e)\sum_m\left|\sum_k\left[\frac{\langle\varphi_f|T_{1m}^{M}|\varphi_k\rangle}{E_k - E_f - \omega_0}\times\langle\varphi_k|\boldsymbol{D}\cdot\hat{\boldsymbol{z}}|\varphi_i\rangle + \frac{\langle\varphi_f|\boldsymbol{D}\cdot\hat{\boldsymbol{z}}|\varphi_k\rangle}{E_k - E_i + \omega_0}\langle\varphi_k|T_{1m}^{M}|\varphi_i\rangle\right]\right|^2, \tag{B7}$$

where $I_s = cF_0^2/32\pi^2$ is the spectral intensity. The above rate is equivalent to the EB excitation rate given in Eq. (1) of Ref. [38] [which uses the nuclear reduced matrix element $|\langle I_g||M_1^M||I_e\rangle|^2$ instead of the reduced transition probability $B(M1, g\to e)$, and averages over initial electronic states and sums over final electronic states].

[1] P. Walker and G. Dracoulis, Energy traps in atomic nuclei, Nature (London) **399**, 35 (1999).

[2] J. J. Carroll, S. A. Karamian, L. A. Rivlin, and A. A. Zadernovsky, X-ray-driven gamma emission, Hyperfine Interact. **135**, 3 (2001).

[3] A. A. Zadernovsky and J. J. Carroll, Non-radiative triggering of long-lived nuclear isomers, Hyperfine Interact. **143**, 153 (2002).

[4] A. Pálffy, J. Evers, and C. H. Keitel, Isomer triggering via nuclear excitation by electron capture, Phys. Rev. Lett. **99**, 172502 (2007).

[5] Y. Wu, C. H. Keitel, and A. Pálffy, ^{93m}Mo isomer depletion via beam-based nuclear excitation by electron capture, Phys. Rev. Lett. **122**, 212501 (2019).

[6] C. S. Cutler, H. M. Hennkens, N. Sisay, S. Huclier-Markai, and S. S. Jurisson, Radiometals for combined imaging and therapy, Chem. Rev. **113**, 858 (2013).

[7] P. Walker and Z. Podolyák, 100 years of nuclear isomers—then and now, Phys. Scr. **95**, 044004 (2020).

[8] L. A. Kroger and C. W. Reich, Features of the low-energy level scheme of ^{229}Th as observed in the α-decay of ^{233}U, Nucl. Phys. A **259**, 29 (1976).

[9] C. W. Reich and R. G. Helmer, Energy separation of the doublet of intrinsic states at the ground state of ^{229}Th, Phys. Rev. Lett. **64**, 271 (1990).

[10] R. G. Helmer and C. W. Reich, An excited state of ^{229}Th at 3.5 eV, Phys. Rev. C **49**, 1845 (1994).

[11] B. R. Beck, J. A. Becker, P. Beiersdorfer, G. V. Brown, K. J. Moody, J. B. Wilhelmy, F. S. Porter, C. A. Kilbourne, and R. L. Kelley, Energy splitting of the ground-state doublet in the nucleus ^{229}Th, Phys. Rev. Lett. **98**, 142501 (2007).

[12] B. Seiferle, L. von der Wense, P. V. Bilous, I. Amersdorffer, C. Lemell, F. Libisch, S. Stellmer, T. Schumm, C. E. Düllmann, A. Pálffy *et al.*, Energy of the ^{229}Th nuclear clock transition, Nature (London) **573**, 243 (2019).

[13] L. von der Wense, B. Seiferle, M. Laatiaoui, J. B. Neumayr, H.-J. Maier, H.-F. Wirth, C. Mokry, J. Runke, K. Eberhardt, C. E. Düllmann *et al.*, Direct detection of the ^{229}Th nuclear clock transition, Nature (London) **533**, 47 (2016).

[14] J. Thielking, M. V. Okhapkin, P. Glowacki, D. M. Meier, L. von der Wense, B. Seiferle, C. E. Düllmann, P. G. Thirolf, and E. Peik, Laser spectroscopic characterization of the nuclear-clock isomer ^{229m}Th, Nature (London) **556**, 321 (2018).

[15] N. Minkov and A. Pálffy, Theoretical predictions for the magnetic dipole moment of ^{229m}Th, Phys. Rev. Lett. **122**, 162502 (2019).

[16] A. Yamaguchi, H. Muramatsu, T. Hayashi, N. Yuasa, K. Nakamura, M. Takimoto, H. Haba, K. Konashi, M. Watanabe, H. Kikunaga *et al.*, Energy of the ^{229}Th nuclear clock isomer determined by absolute γ-ray energy difference, Phys. Rev. Lett. **123**, 222501 (2019).

[17] T. Sikorsky, J. Geist, D. Hengstler, S. Kempf, L. Gastaldo, C. Enss, C. Mokry, J. Runke, C. E. Dullmann, P. Wobrauschek *et al.*, Measurement of the ^{229}Th isomer energy with a magnetic microcalorimeter, Phys. Rev. Lett. **125**, 142503 (2020).

[18] E. Peik and C. Tamm, Nuclear laser spectroscopy of the 3.5 eV transition in ^{229}Th, Europhys. Lett. **61**, 181 (2003).

[19] E. Peik, K. Zimmermann, M. Okhapkin, and C. Tamm, in *Proceedings of the 7th Symposium on Frequency Standards and Metrology*, edited by L. Maleki (World Scientific, Singapore, 2009), pp. 532–538.

[20] W. G. Rellergert, D. DeMille, R. R. Greco, M. P. Hehlen, J. R. Torgerson, and E. R. Hudson, Constraining the evolution of the fundamental constants with a solid-state optical frequency reference based on the ^{229}Th nucleus, Phys. Rev. Lett. **104**, 200802 (2010).

[21] C. J. Campbell, A. G. Radnaev, A. Kuzmich, V. A. Dzuba, V. V. Flambaum, and A. Derevianko, Single-ion nuclear clock for metrology at the 19th decimal place, Phys. Rev. Lett. **108**, 120802 (2012).

[22] V. V. Flambaum, Enhanced effect of temporal variation of the fine structure constant and the strong interaction in ^{229}Th, Phys. Rev. Lett. **97**, 092502 (2006).

[23] J. C. Berengut, V. A. Dzuba, V. V. Flambaum, and S. G. Porsev, Proposed experimental method to determine α sensitivity of splitting between ground and 7.6 eV isomeric states in ^{229}Th, Phys. Rev. Lett. **102**, 210801 (2009).

[24] P. Fadeev, J. C. Berengut, and V. V. Flambaum, Sensitivity of ^{229}Th nuclear clock transition to variation of the fine-structure constant, Phys. Rev. A **102**, 052833 (2020).

[25] L. von der Wense and B. Seiferle, The ^{229}Th isomer: Prospects for a nuclear optical clock, Eur. Phys. J. A **56**, 277 (2020).

[26] E. Peik, T. Schumm, M. S. Safronova, A. Pálffy, J. Weitenberg, and P. G. Thirolf, Nuclear clocks for testing fundamental physics, Quantum Sci. Technol. **6**, 034002 (2021).

[27] J. Jeet, C. Schneider, S. T. Sullivan, W. G. Rellergert, S. Mirzadeh, A. Cassanho, H. P. Jenssen, E. V. Tkalya, and E. R. Hudson, Results of a direct search using synchrotron radiation for the low-energy ^{229}Th nuclear isomeric transition, Phys. Rev. Lett. **114**, 253001 (2015).

[28] A. Yamaguchi, M. Kolbe, H. Kaser, T. Reichel, A. Gottwald, and E. Peik, Experimental search for the low-energy nuclear transition in ^{229}Th with undulator radiation, New J. Phys. **17**, 053053 (2015).

[29] E. Peik and M. Okhapkin, Nuclear clocks based on resonant excitation of γ-transitions, C. R. Phys. **16**, 516 (2015).

[30] S. Stellmer, G. Kazakov, M. Schreitl, H. Kaser, M. Kolbe, and T. Schumm, Attempt to optically excite the nuclear isomer in ^{229}Th, Phys. Rev. A **97**, 062506 (2018).

[31] T. Masuda, A. Yoshimi, A. Fujieda, H. Fujimoto, H. Haba, H. Hara, T. Hiraki, H. Kaino, Y. Kasamatsu, S. Kitao *et al.*, X-ray pumping of the ^{229}Th nuclear clock isomer, Nature (London) **573**, 238 (2019).

[32] E. V. Tkalya, A. N. Zherikhin, and V. I. Zhudov, Decay of the low-energy nuclear isomer ^{229}Th^{m}($3/2^{+}$, 3.5 ± 1.0 eV) in solids (dielectrics and metals): A new scheme of experimental research, Phys. Rev. C **61**, 064308 (2000).

[33] A. Ya. Dzyublik, G. Gosselin, V. Mèot, and P. Morel, Role of screening in Coulomb excitation of nuclei by electrons in hot plasma, Europhys. Lett. **102**, 62001 (2013).

[34] E. V. Tkalya, Excitation of ^{229m}Th at inelastic scattering of low energy electrons, Phys. Rev. Lett. **124**, 242501 (2020).

[35] H. Zhang, W. Wang, and X. Wang, Nuclear excitation cross section of ^{229}Th via inelastic electron scattering, Phys. Rev. C **106**, 044604 (2022).

[36] H. Zhang and X. Wang, Theory of isomeric excitation of ^{229}Th via electronic processes, Front. Phys. **11**, 1166566 (2023).

[37] E. V. Tkalya, Excitation of low-lying isomer level of the nucleus ^{229}Th by optical photons, JETP Lett. **55**, 211 (1992).

[38] S. G. Porsev, V. V. Flambaum, E. Peik, and C. Tamm, Excitation of the isomeric ^{229m}Th nuclear state via an electronic bridge process in ^{229}Th^{+}, Phys. Rev. Lett. **105**, 182501 (2010).

[39] P. V. Borisyuk, N. N. Kolachevsky, A. V. Taichenachev, E. V. Tkalya, I. Yu. Tolstikhina, and V. I. Yudin, Excitation of the low-energy ^{229m}Th isomer in the electron bridge process via the continuum, Phys. Rev. C **100**, 044306 (2019).

[40] P. V. Bilous, H. Bekker, J. C. Berengut, B. Seiferle, L. von der Wense, P. G. Thirolf, T. Pfeifer, J. R. Crespo LópezUrrutia, and A. Pálffy, Electronic bridge excitation in highly charged ^{229}Th ions, Phys. Rev. Lett. **124**, 192502 (2020).

[41] B. S. Nickerson, M. Pimon, P. V. Bilous, J. Gugler, K. Beeks, T. Sikorsky, P. Mohn, T. Schumm, and A. Pálffy, Nuclear excitation of the ^{229}Th isomer via defect states in doped crystals, Phys. Rev. Lett. **125**, 032501 (2020).

[42] A. Y. Dzyublik, Excitation of ^{229m}Th in the electron bridge via continuum, as a scattering process, Phys. Rev. C **102**, 024604 (2020).

[43] A. Y. Dzyublik, Quasiclassical theory of ^{229m}Th excitation by laser pulses via electron bridges, Phys. Rev. C **106**, 064608 (2022).

[44] P. V. Bilous, N. Minkov, and A. Pálffy, Electric quadrupole channel of the 7.8 eV ^{229}Th transition, Phys. Rev. C **97**, 044320 (2018).

[45] J. Feng, W. Wang, C. Fu, L. Chen, J. Tan, Y. Li, J. Wang, Y. Li, G. Zhang, Y. Ma *et al.*, Femtosecond pumping of nuclear isomeric states by the Coulomb collision of ions with quivering electrons, Phys. Rev. Lett. **128**, 052501 (2022).

[46] J. Qi, H. Zhang, and X. Wang, Isomeric excitation of ^{229}Th in laser-heated clusters, Phys. Rev. Lett. **130**, 112501 (2023).

[47] W. Wang, J. Zhou, B. Liu, and X. Wang, Exciting the isomeric ^{229}Th nuclear state via laser-driven electron recollision, Phys. Rev. Lett. **127**, 052501 (2021).

[48] X. Wang, Nuclear excitation of ^{229}Th induced by laser-driven electron recollision, Phys. Rev. C **106**, 024606 (2022).

[49] K. C. Kulander, K. J. Schafer, and J. L. Krause, in *Super-Intense Laser-Atom Physics*, edited by B. Piraux, A. L'Huillier, and K. Rzazewski (Plenum, New York, 1993).

[50] K. J. Schafer, B. Yang, L. F. DiMauro, and K. C. Kulander, Above threshold ionization beyond the high harmonic cutoff, Phys. Rev. Lett. **70**, 1599 (1993).

[51] P. B. Corkum, Plasma perspective on strong field multiphoton ionization, Phys. Rev. Lett. **71**, 1994 (1993).

[52] A. McPherson, G. Gibson, H. Jara, U. Johann, T. S. Luk, I. A. McIntyre, K. Boyer, and C. K. Rhodes, Studies of multiphoton production of vacuum-ultraviolet radiation in the rare gases, J. Opt. Soc. Am. B **4**, 595 (1987).

[53] M. Ferray, A. L'Huillier, X. F. Li, L. A. Lompre, G. Mainfray, and C. Manus, Multiple-harmonic conversion of 1064 nm radiation in rare gases, J. Phys. B **21**, L31 (1988).

[54] J. Seres, E. Seres, A. J. Verhoef, G. Tempea, C. Streli, P. Wobrauschek, V. Yakovlev, A. Scrinzi, C. Spielmann, and F. Krausz, Source of coherent kiloelectronvolt x-rays, Nature (London) **433**, 596 (2005).

[55] B. Walker, B. Sheehy, L. F. DiMauro, P. Agostini, K. J. Schafer, and K. C. Kulander, Precision measurement of strong field double ionization of helium, Phys. Rev. Lett. **73**, 1227 (1994).

[56] S. Palaniyappan, A. DiChiara, E. Chowdhury, A. Falkowski, G. Ongadi, E. L. Huskins, and B. C. Walker, Ultrastrong field ionization of $Ne^{n+}(n \leqslant 8)$: Rescattering and the role of the magnetic field, Phys. Rev. Lett. **94**, 243003 (2005).

[57] W. Becker, X. Liu, P. J. Ho, and J. H. Eberly, Theories of photoelectron correlation in laser-driven multiple atomic ionization, Rev. Mod. Phys. **84**, 1011 (2012).

[58] T. Morishita, A. T. Le, Z. J. Chen, and C. D. Lin, Accurate retrieval of structural information from laser-induced photoelectron and high-order harmonic spectra by few-cycle laser pulses, Phys. Rev. Lett. **100**, 013903 (2008).

[59] C. I. Blaga, J. Xu, A. D. DiChiara, E. Sistrunk, K. Zhang, P. Agostini, T. A. Miller, L. F. DiMauro, and C. D. Lin, Imaging ultrafast molecular dynamics with laser-induced electron diffraction, Nature (London) **483**, 194 (2012).

[60] B. Wolter, M. G. Pullen, A.-T. Le, M. Baudisch, K. Doblhoff-Dier, A. Senftleben, M. Hemmer, C. D. Schröter, J. Ullrich, T. Pfeiffer *et al.*, Ultrafast electron diffraction imaging of bond breaking in di-ionized acetylene, Science **354**, 308 (2016).

[61] F. Krausz and M. Ivanov, Attosecond physics, Rev. Mod. Phys. **81**, 163 (2009).

[62] K. Zhao, Q. Zhang, M. Chini, Y. Wu, X. Wang, and Z. Chang, Tailoring a 67 attosecond pulse through advantageous phase-mismatch, Opt. Lett. **37**, 3891 (2012).

[63] J. Li, X. Ren, Y. Yin, K. Zhao, A. Chew, Y. Cheng, E. Cunningham, Y. Wang, S. Hu, Y. Wu *et al.*, 53-attosecond X-ray pulses reach the carbon K-edge, Nat. Commun. **8**, 186 (2017).

[64] T. Gaumnitz, A. Jain, Y. Pertot, M. Huppert, I. Jordan, F. Ardana-Lamas, and H. J. Wörner, Streaking of 43-attosecond soft-x-ray pulses generated by a passively CEP-stable mid-infrared driver, Opt. Express **25**, 27506 (2017).

[65] A. V. Andreev, A. B. Savel'ev, S. Yu. Stremoukhov, and O. A. Shoutova, Nuclear isomer excitation in ^{229}Th atoms by superintense laser fields, Phys. Rev. A **99**, 013422 (2019).

[66] W. Wang, H. Zhang, and X. Wang, Strong-field atomic physics meets ^{229}Th nuclear physics, J. Phys. B **54**, 244001 (2021).

[67] C. Schwartz, Theory of hyperfine structure, Phys. Rev. **97**, 380 (1955).

[68] W. R. Johnson, *Atomic Structure Theory: Lectures on Atomic Physics* (Springer, Berlin, 2007).

[69] A. Y. Dzyublik, Triggering of nuclear isomers by X-ray laser, JETP Lett. **92**, 130 (2010).

[70] V. L. Lyuboshitz, V. A. Onishchuk, and M. I. Podgoretskij, Some interference effects due to the mixing of quantum levels by external fields, Sov. J. Nucl. Phys. **3**, 420 (1966).

[71] F. F. Karpeshin, S. Wycech, I. M. Band, M. B. Trzhaskovskaya, M. Pfützner, and J. Żylicz, Rates of transitions between the hyperfine-splitting components of the ground-state and the 3.5 eV isomer in $^{229}Th^{89+}$, Phys. Rev. C **57**, 3085 (1998).

[72] K. Pachucki, S. Wycech, J. Żylicz, and M. Pfützner, Nuclear-spin mixing oscillations in $^{229}Th^{89+}$, Phys. Rev. C **64**, 064301 (2001).

[73] K. Beloy, Hyperfine structure in $^{229g}Th^{3+}$ as a probe of the $^{229g}Th \rightarrow {}^{229m}Th$ nuclear excitation energy, Phys. Rev. Lett. **112**, 062503 (2014).

[74] E. V. Tkalya and A. V. Nikolaev, Magnetic hyperfine structure of the ground-state doublet in highly charged ions $^{229}Th^{89+,87+}$ and the Bohr-Weisskopf effect, Phys. Rev. C **94**, 014323 (2016).

[75] E. V. Tkalya, Anomalous magnetic hyperfine structure of the ^{229}Th ground-state doublet in muonic atoms, Phys. Rev. A **94**, 012510 (2016).

[76] V. M. Shabaev, D. A. Glazov, A. M. Ryzhkov, C. Brandau, G. Plunien, W. Quint, A. M. Volchkova, and D. V. Zinenko, Ground-State g factor of highly charged ^{229}Th ions: An access to the M1 transition probability between the isomeric and ground nuclear sates, Phys. Rev. Lett. **128**, 043001 (2022).

[77] N. Minkov and A. Pálffy, ^{229m}Th isomer from a nuclear model perspective, Phys. Rev. C **103**, 014313 (2021).

[78] M. V. Ammosov, N. B. Delone, and V. P. Krainov, Tunnel ionization of complex atoms and of atomic ions in an alternating electromagnetic field, Sov. Phys. JETP **64**, 1191 (1986).

[79] K. C. Kulander, Multiphoton ionization of hydrogen: A time-dependent theory, Phys. Rev. A **35**, 445(R) (1987).

[80] M. Awasthi, Y. V. Vanne, A. Saenz, A. Castro, and P. Decleva, Single-active-electron approximation for describing molecules in ultrashort laser pulses and its application to molecular hydrogen, Phys. Rev. A **77**, 063403 (2008).

[81] A.-T. Le, H. Wei, C. Jin, and C. D. Lin, Strong-field approximation and its extension for high-order harmonic generation with mid-infrared lasers, J. Phys. B **49**, 053001 (2016).

[82] C. Chang, M. Pelissier, and P. Durand, Regular two-component Pauli-like effective Hamiltonians in Dirac theory, Phys. Scr. **34**, 394 (1986).

[83] E. van Lenthe, E. J. Baerends, and J. G. Snijders, Relativistic regular two-component Hamiltonians, J. Chem. Phys. **99**, 4597 (1993).

[84] E. van Lenthe, E. J. Baerends, and J. G. Snijders, Relativistic total energy using regular approximations, J. Chem. Phys. **101**, 9783 (1994).

[85] F. Salvat and J. M. Fernández-Varea, radial: A Fortran subroutine package for the solution of the radial Schrödinger and Dirac wave equations, Comput. Phys. Commun. **240**, 165 (2019).

[86] G. Yao and S. I. Chu, Generalized pseudospectral methods with mappings for bound and resonance state problems, Chem. Phys. Lett. **204**, 381 (1993).

[87] X. M. Tong and S. I. Chu, Theoretical study of multiple high-order harmonic generation by intense ultrashort pulsed

laser fields: A new generalized pseudospectral time-dependent method, Chem. Phys. **217**, 119 (1997).

[88] S. I. Chu and D. A. Telnov, Beyond the Floquet theorem: Generalized Floquet formalisms and quasienergy methods for atomic and molecular multiphoton processes in intense laser fields, Phys. Rep. **390**, 1 (2004).

[89] S. Amoruso, R. Bruzzese, N. Spinelli, and R. Velotta, Characterization of laser-ablation plasmas, J. Phys. B **32**, R131 (1999).

[90] R. E. Russo, X. L. Mao, J. Yoo, and J. J. Gonzalez, in *Laser-Induced Breakdown Spectroscopy*, edited by J. P. Singh and S. N. Thakur (Elsevier, San Diego, 2007), Chap. 3.